Charge Simulation Method and Surface Charge Computation for Design of High Voltage Devices

Andreas Blaszczyk[1], Frank Messerer[2], Carsten Trinitis[1,3]*

[1]*Technical University of Munich, School of Computation, Information, and Technology, Garching, Germany*
[2]*Technical University of Munich, Professorship of High Voltage Engineering, München, Germany*
[3]*Technical University of Munich, School of Computation, Information, and Technology, Campus Heilbronn, Heilbronn, Germany*
**andreas.blaszczyk@tum.de*

Keywords: DIELECTRIC SIMULATIONS, STREAMER INCEPTION, DISCHARGE PROPAGATION, SURFACE CHARGE ACCUMULATION, WITHSTAND VOLTAGE PREDICTION

Abstract

This paper presents an overview of the charge simulation method (CSM) developments which started at the Technical University of Munich in the 1960s and continue until today. The CSM features and the corresponding formulations created during three major development phases are summarised. Altogether, eight types of equations used in the latest CSM-implementation are presented. The newest surface charging simulation procedure, which is one focus of this paper, has been illustrated by two examples of devices belonging to the medium voltage range: a triple point test arrangement and a silicon coated vacuum interrupter. A comparison of results between computations and a dedicated AC test enabled generalisation of the procedure for simulation of triple points. An evaluation of the extremal saturation charge on the silicon coating has shown its impact on LI-withstand and has indicated possible improvements of the insulation shape. The differences between the 2D CSM results and the results obtained using a 3D Boundary Element Method implementation are discussed.

1 Introduction

The Charge Simulation Method (CSM) was one of the first numerical approaches that enabled an efficient prediction of dielectric performance of high voltage devices based on capacitive, electrostatic 2D-field computations [1], [2]. The pilot CSM applications computed in the 1960s and 1970s were limited to simple test configurations including electrodes with predefined potentials and at most two dielectric materials. In spite of the initial limitations CSM has become a widely used method in both academic and industrial environments [3], [4].

About 20 years later this pioneering phase of CSM development was followed by another phase that allowed to remove limitations imposed by the initial formulation. In fact, the main motivation for starting a new phase was the progress in computer technology. In the 1980s the personal computers and workstations had replaced the inefficient input/output of mainframe computers based on punched cards and hard copy listings of numerical results. A more user friendly graphical visualisation of electric fields became available. A framework for the second phase provided the Venus-project [5] supported by the German government and performed by the Technical Universities Karlsruhe, Munich and Hamburg. The extension and the generalisation of CSM formulation was a useful side effect of the Venus-project [6]. It enabled more complex CSM features including boundaries between multiple solid dielectrics, floating potentials, thin foils, stable triple points, high permittivities, conductive fields, etc.

From the mid of 1990s the focus of CSM developers contributing to the first two phases was moved towards 3D field computations based on the Boundary Element Method (BEM) [7], dielectric optimisation [8], investigation of discharge physics as a foundation for understanding the surface charging phenomena [9] and capacitive-resistive calculations for DC applications [10]. As a consequence, the CSM progress almost came to a standstill. However, the CSM codes developed in the past continued to play an important role in some of the new projects. The first example is the EU-supported Casopt project on BEM-based dielectric optimisation performed between 2009 and 2013 by the Technical Universities Munich and Graz and the University of Cambridge [11]. Another example is the project on gas insulation discharges performed between 2015 and 2018 by Sintef Energy and NTNU Trondheim supported by the Norwegian government [12], [13], [14]. ABB was the industrial partner for both projects. These projects laid a foundation for the third phase of CSM development, which started at the beginning of 2021 by launching a new project named “Elfi” [15]. One of goals of the Elfi project is to implement the surface charging formulation and its application on the computation of the withstand voltage of high voltage devices. The Elfi project is currently supported by TU Munich.

An overview of formulations implemented in all three phases of CSM development, indicated according to the year when they have been created (1970, 1990 and 2020), is presented in section 2. The special focus is on the surface charging, which requires not only additional equations for formulating the new saturation boundary condition but also an iterative identification where this boundary condition should be located. The presented formulations are used in this paper to evaluate the critical impact of the surface charge in two application cases including a triple point test arrangement and a silicon coated vacuum interrupter. The device geometries

have been reused based on benchmark models defined within the Casopt and Sintef projects, but the surface charging aspects have been computed for the first time within the new Elfi project. Section 3 shows for both examples the simulation procedure and the results obtained by using the 2D code implemented in all three CSM development phases. A comparison between the 2D and 3D results presented in Section 4 demonstrates that the 3D analysis may be required to obtain more precise results. The 3D simulation is based on a BEM-formulation presented in [16].

2 CSM Formulation

2.1 Initial Concept. 1970

A discretised CSM model consists of surface elements (strips) representing the boundaries between electrodes and dielectric materials. In the middle of each surface element a representative point, called collocation or contour point, is defined. A discrete charge is located at a certain distance from the surface, which is approximately 1.5 times larger than the length of the corresponding strip, see Fig. 1. For electrode surfaces the discrete charges placed inside electrodes are used to compute potentials and fields in the outer domain G as a superposition of all charges assigned to electrodes. The outer domain is typically an insulating fluid like "Gas" in Fig. 1, but it can be oil, atmospheric air or vacuum. The values q_j of the discrete charges are calculated by solving a system of linear equations formulated for points at electrode surface:

$$\sum_{j\in G} p_{ij} q_j = U \tag{1}$$

where p_{ij} is the potential coefficient between the collocation point i and the discrete charge j. U is the applied voltage.
For dielectric surfaces the discrete charges are placed on both sides of the boundary and therefore 2 equations are formulated for each collocation point between gas (G) and solid dielectric (D). They ensure potential and flux continuity as follows:

$$\sum_{j\in G} p_{ij} q_j = \sum_{j\in D} p_{ij} q_j + \varphi_{refD} \tag{2}$$

$$\varepsilon_G \sum_{j\in G} \boldsymbol{n_i \nabla p_{ij}} q_j + \sigma_i = \varepsilon_D \sum_{j\in D} \boldsymbol{n_i \nabla p_{ij}} q_j \tag{3}$$

where $\boldsymbol{n_i \nabla p_{ij}}$ is the scalar product of the surface normal vector $\boldsymbol{n_i}$ and the derivate of the potential coefficient p_{ij} used in (1) and (2). ε_G and ε_D are permittivities of the gas and the solid dielectric, respectively. φ_{refD} is the reference potential, which is in the initial CSM concept always equal to zero (in contrast to the generalised approach presented later in 2.2). A predefined surface charge density σ_i accumulated on the surface exposed to gas is included here, but in typical applications with clean surfaces should be assumed equal to zero. The expressions $j \in G$ and $j \in D$ denote different sets of charges where the charges assigned to electrodes, typically interpreted as a "free charge", are the common intersection of both sets. The common charges are represented in Fig. 1 by a "+"-symbol. The charges assigned to the interface between dielectrics, occasionally interpreted as "polarisation charges", make the difference between the both sets. These charges are represented in Fig. 1 by an "x"-symbol. The "x"-charges inside the insulator belong to set G, whereas the "x"-charges outside insulator belong to set D. A detailed formulation of CSM with the potential coefficient formulas and their derivates defined for the axisymmetric and 2D-cartesian coordinate systems can be found in handbooks [17].

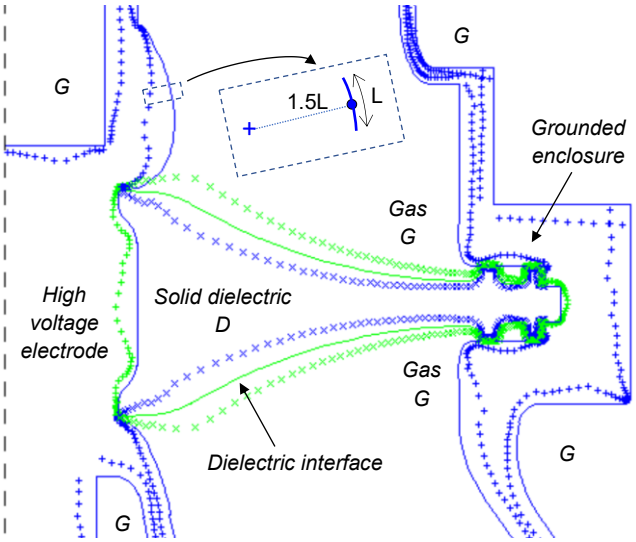

Fig. 1 CSM discretisation for an example of a high voltage switchgear insulator; the zoomed detail shows a surface element with the assigned charge and collocation point.

2.2 Region-Oriented Approach. 1990

The region-oriented CSM breaks with any physical interpretation of the discrete charges. These virtual charges are considered only as an instrument to fulfil the potential continuity and Gauss's law. To each region a unique set of charges is assigned. They are placed directly behind the region boundary, as shown in Fig. 1: charges surrounding the insulator boundary belong the set D (green colour) whereas the rest of charges belong to set G (blue colour). The new concept allows a very flexible discretisation: by subdividing larger regions the charges do not need to be squeezed into thin electrodes provided that different regions are arranged on both sides (infinitely thin foils can be handled!). Based on these features a procedure for automatic discretisation has been elaborated and efficiently used over many years for complex models [18], see example in Fig. 1. Interestingly, the region-oriented concept allows to reuse the rules of charge placement and all equations from (1) to (3) but, as mentioned above, with the changed interpretation of $j \in G$ and $j \in D$. Other equations introduced by the region-oriented approach are presented below.

2.2.1. Flux compensation in a dielectric region: If an unknown reference potential is used within a region to compute a potential value like φ_{refD} in (2), the following additional equation for flux compensation through all boundaries of this region must be included in the equation system:

$$\sum_{i\in D} S_i \sum_{j\in D} \boldsymbol{n_i \nabla p_{ij}} q_j = 0 \tag{4}$$

where S_i is the area of the surface element i. In specific cases this equation should not be formulated for the outer region. For

example, an open air region must preserve a zero potential in infinity. The reference potentials and equation (4) are necessary for the computation of regions with a very high permittivity. They provide a robust instrument for handling conductive fields (used in DC analysis) where the permittivity in (3) is replaced by the electrical conductivity. Typically, the conductivity differences between regions may reach a few orders of magnitude, or for some regions may be equal to zero, which can be reliably handled by the region-oriented CSM.

2.2.2. Flux balance for a floating electrode: Assuming an unknown potential instead of the applied voltage in (*1*) the following additional equation is used to enable solution:

$$\sum_{i,N\in F} S_i \varepsilon_N \sum_{j\in N} \boldsymbol{n_i} \nabla \boldsymbol{p_{ij}} q_j = 0 \tag{5}$$

where the outer integration is performed over all surface elements *i* defining the boundary of the floating electrode *F* and belonging to one of the neighbouring regions *N* (with permittivity ε_N).

2.2.3. Stability equation for triple points: Triple points create a geometrical discontinuity, which may lead to numerical oscillations when increasing the density of discretisation. A stable solution can be achieved by adding an equation ensuring the balance of the flux density exactly at the triple point. For a triple point *t* between an electrode and two dielectric regions *G* and *D* the stabilisation equation is formulated as follows:

$$\varepsilon_G \sum_{j\in G} \boldsymbol{n_{tG}} \nabla \boldsymbol{p_{tj}} q_j + \varepsilon_D \sum_{j\in D} \boldsymbol{n_{tD}} \nabla \boldsymbol{p_{tj}} q_j + \sigma_t = 0 \tag{6}$$

where $\boldsymbol{n_{tG}}$ and $\boldsymbol{n_{tD}}$ are normal vectors pointing to regions *G* and *D* computed by averaging the normal vectors of surface elements connected to the triple point, σ_t is the surface charge density injected from the electrode into both regions at the triple point; σ_t is considered as an additional unknown increasing the degree of freedom of the equation system.

2.3 Surface Charging. 2020

The proposed formulation assumes that the source of charge accumulated on dielectric surfaces is a partial discharge, which may occur during LI or AC tests. The latest experimental investigations and first principle simulations confirmed that the amount of charge as well as dynamics of its accumulation are sufficient to achieve a stage of saturation within nanoseconds [19]. The saturation stage means that no further charge carriers can be deposed on the surface, and this can be reflected by setting the normal field on the charged side (gas side, *G*) to zero:

$$\sum_{j\in G} \boldsymbol{n_i} \nabla \boldsymbol{p_{ij}} q_j = 0 \tag{7}$$

After applying (*7*) to (3) and replacing the predefined σ_i by the unknown saturation charge density σ_{isat} the second equation, can be formulated as follows:

$$\varepsilon_D \sum_{j\in D} \boldsymbol{n_i} \nabla \boldsymbol{p_{ij}} q_j - \sigma_{isat} = 0 \tag{8}$$

A localisation of the surface elements *i*, to which the new saturation boundary condition should be applied, is essential. We assume that the saturation will occur around a point where the discharge arrives at the dielectric surface (called "seed" point). Initially, the boundary condition (*7*), (*8*) is assigned to a larger surface area connected to the seed point, which is supposed to be affected by creeping sparks. However, the saturation charge obtained as a solution may include surface elements for which the polarity of σ_{isat} is opposite to the polarity of the discharge arriving at the seed point. For such elements the initial boundary condition (*7*), (*8*) is changed to (3) (with zero σ_i) and the solution of the whole equation system is repeated iteratively until all calculated σ_{isat} values have the same polarity as the discharge. More details on this iterative procedure can be found in [20].

3 Application examples

3.1 Triple Point Test Arrangement

A dedicated test arrangement for investigation of triple points has been built and measured under AC load in the scope of the Sintef project [12]. The critical triple points have been created at the interface between a cylindrical insulator and two disk electrodes as shown by the cross section in Fig. 2a. It is a typical configuration of mechanical bushings transferring the torque from a grounded drive to the contacts of disconnectors or load breaks in medium voltage switchgear. The focus is on the triple point at the grounded electrode, which is more critical than its counterpart at the active electrode due to insufficient shielding. The simulation procedure is divided into the three following stages:

3.1.1. Stage 1. Background field: The computation of the background field is based on equations (*1*)-(4) and (*6*). The goal is identification of critical surface spots with the maximum field strength and evaluation of inception voltage U_{inc} based on streamer trajectories calculated as field lines started from the critical spots, see Fig. 2b. The effective ionisation coefficients and the streamer constants used for the calculation of U_{inc} are based on empirical formulas [21] proven over years in many engineering simulations [22]. The simulation of U_{inc} at triple points is not straightforward due to a very specific field distribution in the narrow space between the insulator and electrode, see $E_{background}$ in Fig. 2c. The maximum field is located very closely to the triple point where the air space is not sufficient for electron avalanches to create a self-propagating streamer [21]. Even if the avalanches continue along the dielectric interface the tangential field strength is not high enough to fulfil the inception criterion. Therefore, U_{inc} is calculated for other field lines with a lower field strength but with a larger length that enables inception. The critical field line with the lowest inception voltage $U_{incBackground}$ = 102.7 kV as well as the corresponding "seed" point of negative polarity have been localised as shown in Fig. 2bc.

3.1.2. Stage 2. Saturation: In this example the initial location of the saturation boundary condition (*7*), (*8*) can be applied to the whole insulator surface. Based on the negative seed point, the initial charge location has been iteratively reduced to a surface patch below the mid of the insulator as shown in the sketch in Fig. 2a. The value of the saturation charge density is

of interest mainly in the close vicinity of the triple point, which is shown as σ_{sat} in Fig. 2c. In stage 2, due to the accumulated charge the air space of the triple point becomes a field free region where any discharge activity is suppressed.

3.1.3. Stage 3. Restrikes: This stage is reached after the peak value of the applied voltage is changed from +100 kV to -100 kV (after the half of AC period). For the CSM computations the same equations as in the Stage 1 are used. The only changes are the opposite sign of the applied voltage in (*1*) and the replacement of σ_i=0 in (3) by σ_{isat} obtained in the stage 2. In the restrike stage the field strength is almost doubled since the negative electrode is supported by the negative charge accumulated on the dielectric surface. This is reflected in the maximum field strength of 47.8 kV/mm and the low inception level $U_{incRestrike}$ = 53.3 kV as shown in Fig. 2c.

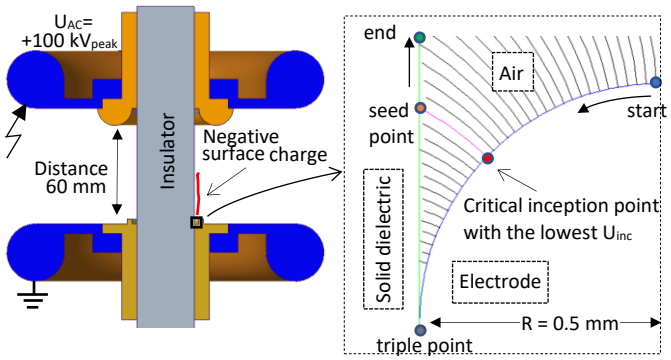

a *b*

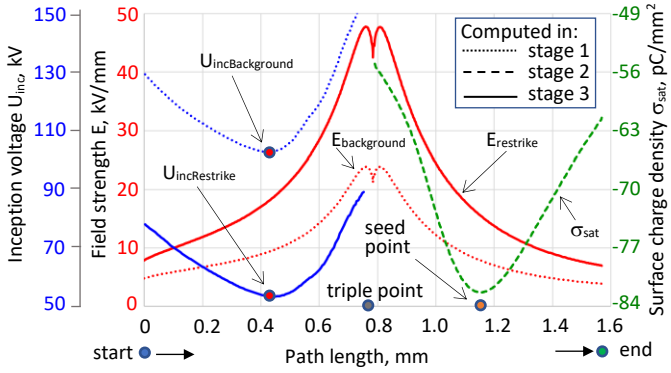

c

Fig. 2 (a) Cross section through the triple point test arrangement; (b) zoomed vicinity of triple point with calculated field lines and the surface evaluation path; (c) distribution of field strength, surface charge density and inception voltage along the surface evaluation path.

The three-stage-procedure has been applied to four tested configurations, where the distance between electrodes was varied between 50 and 80 mm, Fig. 3a. The 50% AC-breakdown voltage has been compared with the simulated minimum inception voltages $U_{incBackground}$ and $U_{incRestrike}$ in Fig. 3b. While $U_{incBackground}$ is evidently a too optimistic prediction of a breakdown, $U_{incRestrike}$ can be considered as a safe prediction below which no breakdown occurs. The restrike stage gives a pessimistic prediction based on an assumption that contaminations, particles, surface protrusions or gaps between the insulator and electrode will lead to an initial inception in stage 1. Once it happens the inception level comes down to $U_{incRestrike}$ (which can be roughly approximated by $U_{incRestrike}=U_{incBackground}/2$). This kind of prediction is based on the calculation of an idealised triple point geometry. However, with a conservative assumption of a restrike, the proposed approach could provide a safety margin required in engineering simulations. Refinements of this approach will be subject to future research.

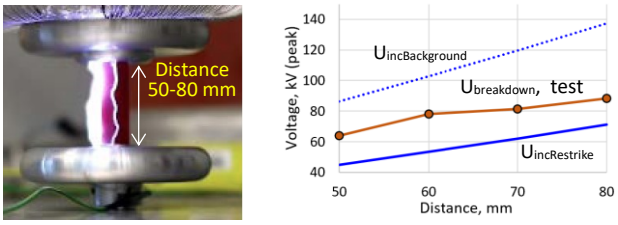

a *b*

Fig. 3 (a) Breakdown in the test arrangement during AC test, (b) Comparison between simulated (U_{inc}) and measured ($U_{breakdown}$) voltages.

3.2 Silicon Coated Vacuum Interrupter

In contrast to the lightning impulse (LI) tests of standalone vacuum interrupters (VI) the similar tests performed for the same VIs installed inside of switchgear compartments show a bigger failure rate. This particularly holds true for voltage levels ≥ 24 kV, based on practical experience of various manufacturers of medium voltage devices. One explanation is the surface charge accumulated on the silicon surface, which may appear due to discharges initiated by support elements, barriers, particles, etc. The example shown in Fig. 4 illustrates the effect of the surface charge for a 24 kV silicon coated VI during an LI test with +125 kV. With an a priori defined negative polarity seed point (close to a high field surface spot) the saturation boundary condition (*7*), (*8*) can be applied to the whole interface between silicon and gas. The iterative procedure described in section 2.3 obtains the values of the negative surface charge and the location where it is accumulated, see sketch in Fig. 4a.

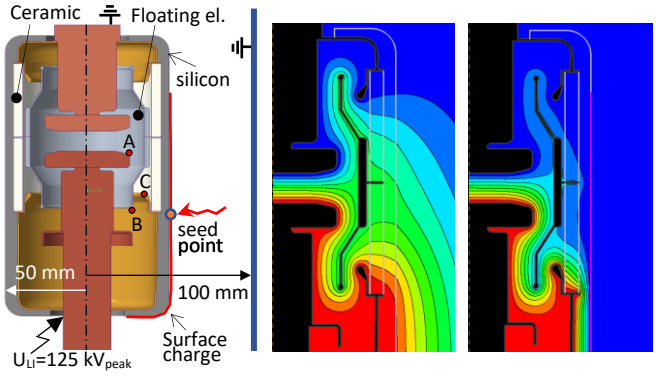

a *b* *c*

Fig. 4 (a) Vacuum interrupter cross section with accumulated surface charge layer and critical points A,B,C; (b) and (c) potential distribution during the peak of the LI test without and with surface charge accumulated on silicon surface.

Due to capacitive coupling of the charge layer with the floating electrode inside of VI the value of its floating potential will be decreased from 54.3 kV to 25.6 kV which happens during the LI peak. Consequently, the field strength at critical spots A and B will be increased by 40% and at spot C by 74%. The last one is exposed not only to the floating electrode but also to the location where the negative saturation charge density has reached the extremal value of -440 pC/mm^2 (close to the location of the seed point in Fig. 4a). This may seriously degrade the VI withstand performance compared to a surface charge free configuration.

4 Comparison 2D CSM versus 3D BEM

The CSM formulation has been implemented for solving 2D models, which significantly narrows down its application range to simplified cases. Consequently, CSM is mainly used for dedicated experimental models or initial evaluation of component behaviour. Trials of implementing equations (*1*)-(*8*) by using discrete charges in 3D turned out to be not robust enough for solving complex models. Therefore, effort has been invested into implementation of an equivalent indirect BEM formulation that uses very similar equations but instead of discrete charges q_j the virtual charge densities σ_j defined directly at model surfaces are used [7],[16]. The term "indirect" reflects the fact that the primary solution is not directly the field distribution but (like in case of CSM) the virtual charge that is used in the second step to compute field strength and potential. In this section we apply the indirect BEM implementation to compute both examples from section 3 after introducing 3D geometrical features.

The triple point test arrangement has been designed to enable both the cylindrical and the hexagonal insulator shapes. The last one (Fig. 5a) is typically used for mechanical bushings in switchgear drives. The simulation procedure in 3D includes the same three stages described in subsection 3.1. Similar to the 2D result, the iteratively calculated negative saturation charge is limited to the lower part of the insulator, see Fig. 5a.

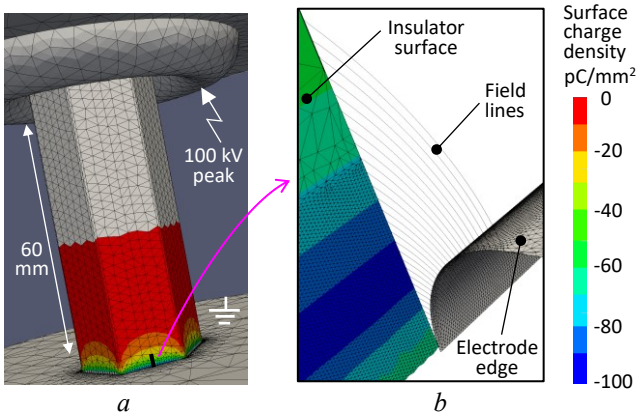

Fig. 5 3D BEM results plot with the negative saturation charge density accumulated on the hexagonal insulator of the triple point test arrangement (a) full view of the insulator, (b) zoomed detail with field lines starting from the inception spots along the midline of the electrode edge. The insulator and electrode surfaces have been cut to enable viewing.

The planar walls of the hexagonal insulator cause the field distribution in the close vicinity of the triple point to oscillate in circumferential direction. The maximum field strength and the saturation charge density reach extremal values in the middle of the planar walls, Fig. 5ab. They exceed the level calculated in the axisymmetric model by approximately 10-15%, However, this increase is not because of the deviations in model geometry. The 2D result for the cylindrical insulator differs only within the range 1-2% from the equivalent 3D-hexagonal result. The major part of the 10-15% difference is due to a higher relative permittivity specified as 5.0 for the hexagonal insulator and 4.6 for the cylindrical. It should be noted that the saturation charge density is directly proportional to the permittivity, which is evident from the equation (*8*). This difference has been confirmed by a slightly lower breakdown voltage measured for the hexagonal insulator [12].

In a 3D simulation model the vacuum interrupter is surrounded by enclosure walls and the grounded neighbouring mid-phase. Replacing the cylindrical enclosure with other grounded elements (while keeping the same distance) does not have any significant effect on saturation charge. The charge accumulation is dominated by the capacitive coupling between the silicon-gas interface and the internal electrodes of the VI. Therefore, a reshaping of this interface by introducing 3D features may be helpful for a reduction of the charged surface area. To illustrate this, we enhanced the silicon coating in the 3D model by adding four axial sheds that are supposed to stop the circumferentially gliding partial discharge and limit the charge accumulation to an area facing only one of the grounded walls, see Fig. 6.

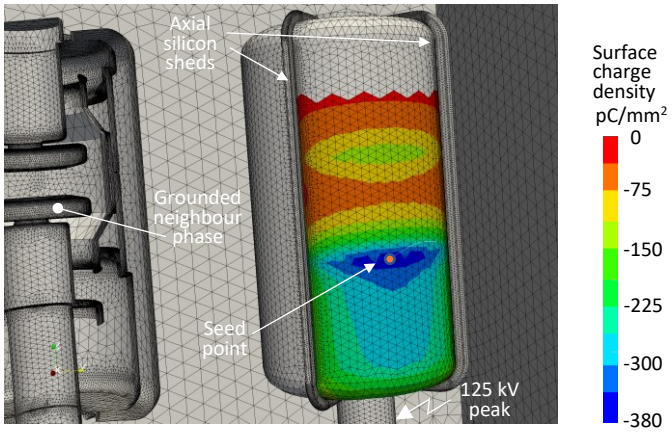

Fig. 6 Saturation charge density computed for a 3D VI-model on the silicon coating with axial sheds: the charging is limited to a surface area less than ¼ of the axisymmetric case.

This result has been iteratively computed based on a single seed point, which specifies where the initial discharge arrives [20]. The reduction of the accumulated charge has a significant impact on the floating electrode, which is at potential of 47.7 kV (only 12 % less than without the surface charge). The growth of the field strength in critical spots A and B is now limited to 11%. The corresponding growth in spot C remains at a relatively high level of 47% since it is affected by the close location of the highest negative surface charge density of -380 pC/mm^2. Further mitigation of the field in the spot C could be achieved by locally increasing the thickness of the coating or

reducing the value of silicon permittivity. This result demonstrates how a device insulation can be optimised for an operation under extremal conditions represented by the saturation charge accumulation.

5 Conclusion

Even 60 years after it was invented, CSM continues to play a pioneering role in the design of high voltage devices. The newest saturation charge formulation extends the traditional CSM functionality scope: an assessment of the highest possible surface charge accumulated due to partial discharges in gases enables an efficient withstand prediction under the extremal operational and test conditions. Traditionally, CSM implementations have been used for 2D models (which can be extracted from a CAD system and automatically discretised) showing good performance**.** For 3D models the use of the indirect BEM formulation including the saturation charge boundary condition is recommended. A combination of both CSM and BEM has been proven to be an efficient simulation environment for dielectric design in high voltage engineering. Current and future research efforts [15] are focusing on development of a new simulation platform**,** which includes elements of discharge physics, optimisation as well as more efficient use of high performance computing features, and making this platform available for the high voltage technology research community.

6 Acknowledgements

The authors dedicate this paper to the memory of Prof. Hans Steinbigler (1934-2021) of TU Munich, who was the pioneer in applying numerical computations in high voltage technology.

7 References

[1] Steinbigler, H.: 'Digitale Berechnung elektrischer Felder', ETZ-A, 1969, pp. 663 – 666 (in German).
[2] Steinbigler, H.: 'The dawn of electric field simulation - a journey through time.', Talk at the closing conference of the Casopt project, https://ellipticfields.com/doc/ElfiDawn.pdf, Baden Switzerland, March 2013.
[3] Moeller, J., Steinbigler, H., Weiss, P.: 'Feldstärkeverlauf auf Abschirmelektroden für ultrahohe Wechselspannungen', ISH München, 1972, pp. 36–44 (in German).
[4] Singer, H., Steinbigler, H., Weiss, P.: 'A Charge Simulation Method for the Calculation of High Voltage Fields', IEEE Trans. Power Appar. & Syst., Vol. 93, pp. 1660-1668, 1974.
[5] Singer, H., Schwab, A.J., Steinbigler, H., et al.: 'VENUS – An open field calculation system with defined data interfaces', Mat. of 7. International Symposium on High Voltage Engineering (ISH), August 1991, Dresden, paper 11.08, vol: Electromagnetic Fields, pp. 39-42
[6] Blaszczyk, A. and Steinbigler H.: 'Region-oriented charge simulation', IEEE Trans. on Magnetics, vol 30, no. 5, September 1994, pp. 2924–2927.
[7] Andjelic, Z., Krstajic B., Milojkovic, S., et al.: 'Integral methods for the calculation of electric fields', Research Center Jülich, Scientific Series of the Int. Bureau, 1992
[8] Trinitis, C.: 'Feldoptimierung von dreidimensionalen Isoliersystemen in der Hochspannungstechnik', PhD. Thesis, VDI Series No. 242, TU Munich, 1997 (in German).
[9] Blaszczyk, A., Böhme, H., Pedersen A., et al.: 'Simulation based spark-over prediction in the medium voltage range', International Symposium on High Voltage Engineering (ISH), Bangalore 2001.
[10] Messerer, F., Boeck, W., Steinbigler, H., Chakravorti, S.: 'Enhanced Field Calculation for HVDC GIS', Gaseous Dielectrics IX, pp. 473-483, Maryland, 2001.
[11] Casopt: https://cordis.europa.eu/project/id/230224, EU-project, Munich, Graz, Cambridge, Baden (CH), 2009-2013
[12] Stoa-Aanensen, N. S.: 'Initial testing of breakdown voltage, 50 Hz stresses on triple junction setup': Report AN-15.14.64, SINTEF Energy Research. Trondheim, 2015.
[13] Pedersen A., Blaszczyk A.: 'An engineering approach to computational prediction of breakdown in air with surface charging effects,' IEEE Trans. on Dielectrics and Electrical Insulation, vol. 24, no. 5, Oct. 2017.
[14] Meyer, H. K.: 'Dielectric barriers under lightning impulse stress', PhD. Diss., No. 106, NTNU Trondheim 2019
[15] Elfi Project Website, http://ellipticfields.com, München-Zürich, July 2021.
[16] Blaszczyk, A., Christen, T., Meyer, H. K., at al.: 'Surface charging formulations for engineering applications. Validation by experiments and transient models', Scientific Computing in Electrical Engineering SCEE 2018, Taormina, Springer Nature 2020.
[17] Messerer, F.: 'Hochspannungsfelder', Handbook of TU Munich, 1st Edition 2021 (in German).
[18] Nilsson, H., Wolpert, P.: 'Automatic boundary discretization for the region-oriented charge simulation', M.Sc. Graduation Project, Royal Institute of Technology, NADA Dept., TRITA-NA-E9272, Stockholm 1992.
[19] Meyer, H.K., Mauseth, F., Marskar, R. et al.: 'Streamer and surface charge dynamics in non-uniform air gaps with a dielectric barrier', IEEE Trans. on Dielectrics and Electrical Insulation, Vol. 26, No. 4, August 2019.
[20] Blaszczyk, A., Morelli, E., Homayonifar, P.: 'Surface Charging Models for Prediction of Dielectric Withstand in Medium Voltage Range', IEEE Trans. on Magnetics, Vol. 57, June 2021.
[21] Petcharaks, K.: 'Applicability of the Streamer Breakdown Criterion to Inhomogeneous Gas Gaps', Ph. D. Thesis No. 11192, ETH Zurich, 1995.
[22] Blaszczyk, A., Christen, T., Kaufmann, P., et al.: 'Virtual High Voltage Lab. Computer based dielectric testing', ABB Review 2021/2.